

This work was written as part of one of the author's official duties as an Employee of the United States Government and is therefore a work of the United States Government. In accordance with 17 U.S.C. 105, no copyright protection is available for such works under U.S. Law. Access to this work was provided by the University of Maryland, Baltimore County (UMBC) ScholarWorks@UMBC digital repository on the Maryland Shared Open Access (MD-SOAR) platform.

Please provide feedback

Please support the ScholarWorks@UMBC repository by emailing scholarworks-group@umbc.edu and telling us what having access to this work means to you and why it's important to you. Thank you.

Formation of large ($\simeq 100\ \mu\text{m}$) ice crystals near the tropical tropopause

E. J. Jensen¹, L. Pfister¹, T. V. Bui¹, P. Lawson², B. Baker², Q. Mo², D. Baumgardner³, E. M. Weinstock⁴, J. B. Smith⁴, E. J. Moyer⁴, T. F. Hanisco⁴, D. S. Sayres⁴, J. M. St. Clair⁴, M. J. Alexander⁵, O. B. Toon⁶, and J. A. Smith⁶

¹NASA Ames Research Center, Moffett Field, CA, USA

²SPEC Inc., Boulder, CO, USA

³Centro de Ciencias de la Atmosfera, Universidad Nacional Autonoma de Mexico, Circuito Exterior, Mexico

⁴Harvard University, Cambridge, MA, USA

⁵Colorado Research Associates, Boulder, CO, USA

⁶University of Colorado, Boulder, CO, USA

Received: 27 March 2007 – Published in Atmos. Chem. Phys. Discuss.: 10 May 2007

Revised: 28 August 2007 – Accepted: 12 October 2007 – Published: 18 March 2008

Abstract. Recent high-altitude aircraft measurements with in situ imaging instruments indicated the presence of relatively large ($\simeq 100\ \mu\text{m}$ length), thin (aspect ratios of $\simeq 6:1$ or larger) hexagonal plate ice crystals near the tropical tropopause in very low concentrations ($<0.01\ \text{L}^{-1}$). These crystals were not produced by deep convection or aggregation. We use simple growth-sedimentation calculations as well as detailed cloud simulations to evaluate the conditions required to grow the large crystals. Uncertainties in crystal aspect ratio leave a range of possibilities, which could be constrained by knowledge of the water vapor concentration in the air where the crystal growth occurred. Unfortunately, water vapor measurements made in the cloud formation region near the tropopause with different instruments ranged from $<2\ \text{ppmv}$ to $\simeq 3.5\ \text{ppmv}$. The higher water vapor concentrations correspond to very large ice supersaturations (relative humidities with respect to ice of about 200%). If the aspect ratios of the hexagonal plate crystals are as small as the image analysis suggests ($6:1$, see companion paper (Lawson et al., 2008)) then growth of the large crystals before they sediment out of the supersaturated layer would only be possible if the water vapor concentration were on the high end of the range indicated by the different measurements ($>3\ \text{ppmv}$). On the other hand, if the crystal aspect ratios are quite a bit larger ($\simeq 10:1$), then H_2O concentrations toward the low end of the measurement range ($\simeq 2\text{--}2.5\ \text{ppmv}$) would suffice to grow the large crystals. Gravity-wave driven temperature and vertical wind perturbations only slightly modify the H_2O concentrations needed to grow the crystals. We find that it would not be possible to grow the

large crystals with water concentrations less than $2\ \text{ppmv}$, even with assumptions of a very high aspect ratio of 15 and steady upward motion of $2\ \text{cm s}^{-1}$ to loft the crystals in the tropopause region. These calculations would seem to imply that the measurements indicating water vapor concentrations less than $2\ \text{ppmv}$ are implausible, but we cannot rule out the possibility that higher humidity prevailed upstream of the aircraft measurements and the air was dehydrated by the cloud formation. Simulations of the cloud formation with a detailed model indicate that homogeneous freezing should generate ice concentrations larger than the observed concentrations ($20\ \text{L}^{-1}$), and even concentrations as low as $20\ \text{L}^{-1}$ should have depleted the vapor in excess of saturation and prevented growth of large crystals. It seems likely that the large crystals resulted from ice nucleation on effective heterogeneous nuclei at low ice supersaturations. Improvements in our understanding of detailed cloud microphysical processes require resolution of the water vapor measurement discrepancies in these very cold, dry regions of the atmosphere.

1 Introduction

Widespread, optically thin, laminar cirrus clouds prevalent near the cold tropical tropopause have attracted considerable interest over the past several years due to their potential role in controlling the water vapor concentration in the stratosphere. Several modeling studies have suggested that these clouds can effectively freeze-dry air crossing the tropical tropopause to the observed lower stratospheric water vapor concentrations (Jensen et al., 1996; Holton and Gettelman, 2001; Gettelman et al., 2002; Jensen and Pfister, 2004;

Correspondence to: E. J. Jensen
(eric.j.jensen@nasa.gov)

Fueglistaler et al., 2005). Stratospheric humidity ultimately affects polar stratospheric cloud formation and polar ozone destruction (Toon et al., 1989; Solomon et al., 1986), as well as gas-phase ozone destruction (Dvorstov and Solomon, 2001). In addition, thin cirrus near the tropopause may significantly affect the Earth's radiation budget as well as the local thermal budget near the tropopause (Comstock et al., 2002).

The inaccessibility of the tropical tropopause region (≈ 16 – 18 km altitude) has limited microphysical measurements of these thin cirrus in the past. During the 2006 CRAVE (Costa Rica Aura Validation Experiment) mission, subvisible cirrus near the tropical tropopause were sampled extensively with an unprecedented array of microphysical instrumentation on-board the NASA WB-57 aircraft. The hydrometeor imaging instruments indicated the presence of relatively large (≈ 80 – $110 \mu\text{m}$) ice crystals only a few hundred meters below the tropopause on multiple flights. (We use the term “tropopause” to refer to the cold point in the vertical temperature profile. Also, we define the tropical tropopause layer (TTL) here as the layer between about 15 and 20 km that has positive radiative heating under clear-sky conditions.)

In this study, we use numerical simulations of crystal growth and sedimentation to investigate the conditions required to form such large crystals. We find that even if the ice concentrations in these clouds were low enough to prevent depletion of vapor due to crystal growth, it is challenging to model the growth of the large crystals, and large ice supersaturations may be required. The degree of supersaturation required to grow the large hexagonal plate crystals depends on their aspect ratios, which appear to be about 6:1 based on analysis of the crystal images presented in a companion paper (Lawson et al., 2008). However, uncertainty associated with blur in the crystal images allows the possibility of somewhat larger aspect ratios. Multiple combinations of water vapor concentrations and aspect ratios would allow growth of the large crystals. We discuss these results with respect to the wide range of TTL water vapor concentrations indicated by the different instruments used in CRAVE. We also evaluate nucleation scenarios that can produce the observed ice crystal number concentrations while still resulting in formation of a small number of large crystals.

In Sect. 2 we describe the measurements indicating large crystals in the TTL cirrus as well as the CRAVE water vapor measurements. Next, we present simple growth-sedimentation calculations used to understand the formation of the observed crystals (Sect. 3). The influence of wave-driven temperature and vertical wind perturbations is discussed in Sect. 4. Simulations of entire vertical profiles of ice crystals and interactions with water vapor are then presented (Sect. 5). Lastly, we present various scenarios for consistency between the range of water vapor concentrations indicated by the measurements and the existence of the large ice crystals (Sect. 6).

2 Ice crystal and water vapor measurements

Given the heights of clouds within the TTL (15–18 km), direct sampling is only possible with specialized, high-altitude aircraft. Only a few such measurements have been made in the past, and only one of these included actual images of the ice crystals. Heymsfield (1986) reported in situ measurements of thin cirrus near the tropical tropopause, using a formvar replicator onboard a WB-57 during the mid-1970s. The ice crystals were mostly trigonal or columnar, with sizes up to $50 \mu\text{m}$. McFarquhar et al. (2000) reported Axially Scattering Spectrometer Probe (ASSP, 2 – $30 \mu\text{m}$) and One-Dimensional Cloud (1DC, 20 – $330 \mu\text{m}$) measurements from the same flight. Crystals larger than $17 \mu\text{m}$ were not detected by the ASSP, but the 1DC occasionally detected crystals with maximum dimensions as large as $50 \mu\text{m}$. However, as discussed by Lawson et al. (2008), these instruments were likely to be incapable of properly sizing crystals in the size range from about 30 to $150 \mu\text{m}$. Peter et al. (2003) reported Forward Scattering Spectrometer (FSSP-300) measurements in an extremely thin cirrus cloud sampled near the tropical tropopause by the Geophysica aircraft. The measurements indicated a distinct mode in the size distribution at about 10 – $12 \mu\text{m}$ diameter, but there was no instrumentation to detect crystals larger than $23 \mu\text{m}$.

Here we present measurements indicating unexpectedly large crystals near the tropical tropopause. Instrumentation on-board the WB-57 during CRAVE for measuring ice crystal sizes and habits included the Cloud Particle Imager (CPI) (Lawson et al., 2001), the 2-Dimensional Stereo probe (2D-S) (Lawson et al., 2006), and the Cloud Aerosol and Precipitation Spectrometer (CAPS) (Baumgardner et al., 2001). The CPI records digital images ($2.3 \mu\text{m}$ pixel size) of crystals that pass through the sample volume. The 2D-S probe captures two-dimensional images of crystals that pass through the sample volume. The 2D-S is an improvement over older optical imaging probes that suffered from slow time response and missed most crystals smaller than $100 \mu\text{m}$ at the airspeeds of jet aircraft. The 2D-S provides actual $10 \mu\text{m}$ particle size resolution at the nominal WB-57F airspeed of 170 m s^{-1} (Lawson et al., 2006). CAPS consists of two instruments: the Cloud Aerosol Spectrometer (CAS) retrieves particle sizes by measuring light scattered off the particles and has an effective size range of 0.5 – $50 \mu\text{m}$; the Cloud Imaging Probe (CIP) is similar to 2D-S except that it has a resolution of $25 \mu\text{m}$ and a slightly slower electronic response time that may limit its size range from 50 to $1550 \mu\text{m}$.

During the CRAVE time period (14 January–11 February, 2006) tropical tropopause temperatures were anomalously cold, particularly during the first three weeks of the mission. Tropopause temperatures measured by the meteorological measurement system (MMS) on the WB-57 were typically around 186 K or less, and the minimum temperature measured was 180.5 K. As a result of these cold temperatures, the TTL was often highly supersaturated with respect to ice and

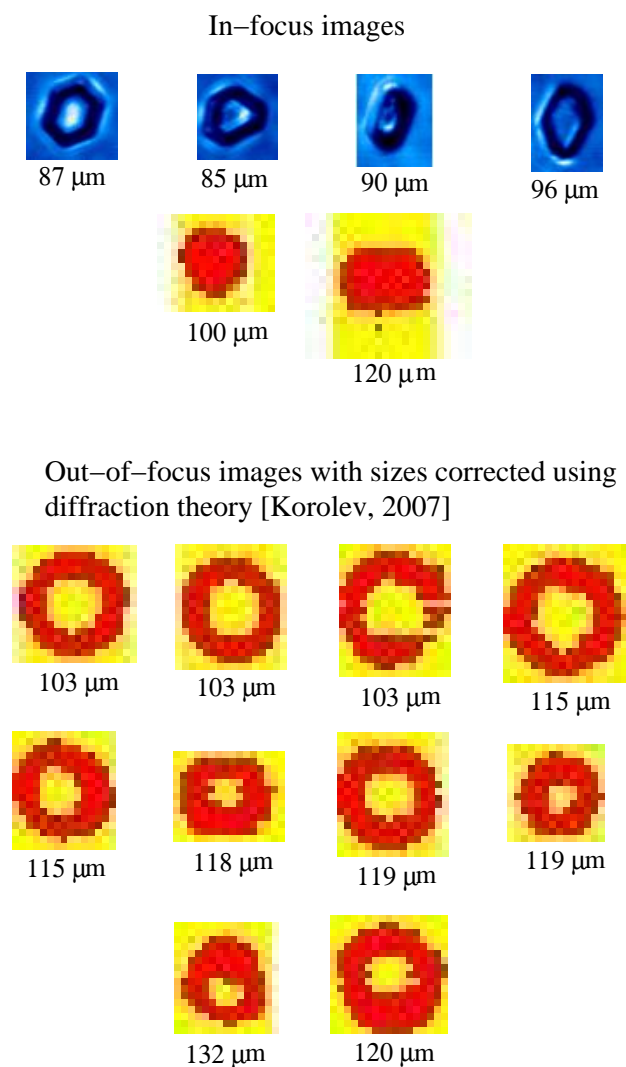


Fig. 1. In-focus CPI images of crystals with maximum dimensions of at least $85\ \mu\text{m}$ and 2D-S images of crystals larger than $100\ \mu\text{m}$ (top) sampled in the TTL cirrus on 1 February are shown. Out-of-focus 2D-S images of large crystals are shown below. The size of these images is corrected using an algorithm based on diffraction theory (see text for details).

optically thin cirrus were sampled on several flights. Lawson et al. (2008) provide a detailed description of the subvisible cirrus properties. On at least four of these flights, relatively large ($>65\ \mu\text{m}$) ice crystals were apparent in the CPI, 2D-S, and CIP images. The large crystals were most prevalent on the flight south from Costa Rica on 1 February while the aircraft was porpoising through the TTL. Low concentrations ($<0.01\ \text{L}^{-1}$) of crystals larger than $65\ \mu\text{m}$ were detected during this time period. Four CPI crystals larger than $85\ \mu\text{m}$ and 12 2D-S images larger than $100\ \mu\text{m}$ were detected (see Fig. 1). One would expect to detect more of the large crystals with 2D-S than with CPI given the larger sample volume

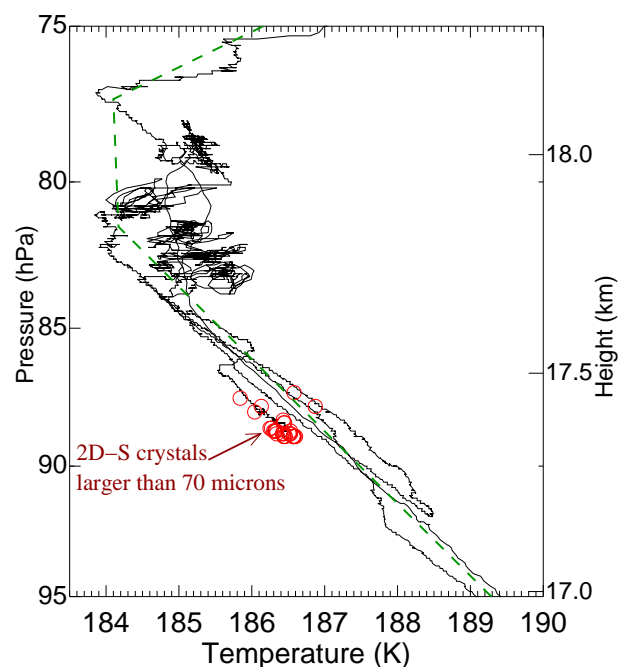


Fig. 2. Temperature versus pressure is shown for the time period when the WB-57 was porpoising through thin cirrus in the tropopause region on 1 February. Red circles indicate the locations where the 2D-S recorded images of crystals with lengths larger than $70\ \mu\text{m}$. The green curve indicates the temperature profile used in growth-sedimentation calculations described below.

of the former (about $10\ \text{L s}^{-1}$). These large crystals were at pressure levels between about 87 and 90 hPa, which was only about 500 m below the tropopause (see Fig. 2).

Most of the 2D-S large-crystal images are out of focus and appear as donuts. The sizes reported for these images have been corrected based on diffraction theory (Lawson et al., 2008; Korolev, 2007). The lengths of the in-focus 2D-S crystals shown in Fig. 1 are 100 and $120\ \mu\text{m}$, and the lengths of the CPI images range from 85 to $96\ \mu\text{m}$; however, the CPI crystals with dimensions $\geq 90\ \mu\text{m}$ were sampled at a somewhat lower altitude ($\approx 95\ \text{hPa}$). The uncertainty in the sizing of the CPI images is at most $5\ \mu\text{m}$. Even for the in-focus 2D-S images, the sizing uncertainty is larger than for the CPI because the pixel size is larger and it is possible that the images are somewhat out of focus without a blank spot appearing in the middle. In a worst-case scenario, the $120\ \mu\text{m}$ in-focus image could be a crystal as small as about $90\ \mu\text{m}$. On the other hand, the digitization error in some cases could lose elements on both sides of the image such that the size could be underestimated by as much as $20\ \mu\text{m}$.

The sizing uncertainty for the out-of-focus 2D-S images is more difficult to quantify. Comparisons between size distributions based on only the in-focus images and only the out-of-focus images that were resized using the Korolev algorithm indicates that the algorithm is doing a reasonable job

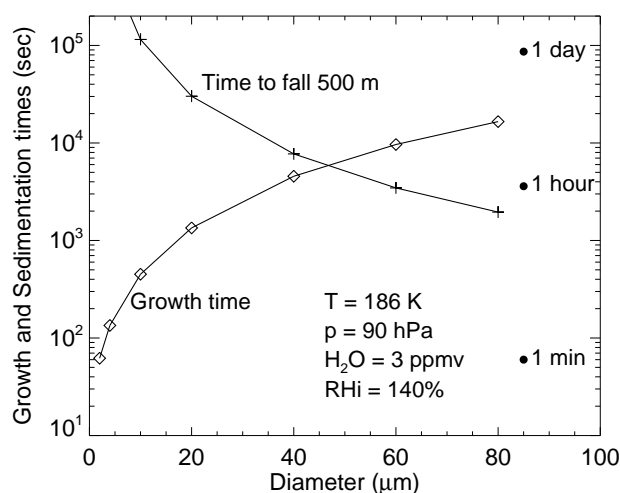


Fig. 3. Crystal growth time and the time to fall 500 m are plotted versus crystal diameter (assuming spheres). (See Sect. 3 for details of growth and sedimentation calculations.) With the assumed temperature (186 K), pressure (90 hPa), and water vapor concentration (3 ppmv), the relative humidity with respect to ice is $\approx 140\%$, and the growth time exceeds the sedimentation time for crystals larger than about 40–50 μm . With higher water vapor concentrations (and larger supersaturations) the growth times will be shorter, allowing growth of larger crystals.

statistically, with at worst about 20% overestimate in the corrected sizes (Lawson et al., 2008). The uncertainty for individual crystals could be larger, but one would not expect it to necessarily be systematic (beyond the apparent high bias of up to 20%). We have 10 out-of-focus images here with corrected sizes greater than 100 μm and 7 with sizes $\geq 115 \mu\text{m}$. We conclude from this analysis that the 2D-S images provide strong evidence for the existence of large (90–100 μm) crystals in the TTL cirrus, and it appears likely that crystals as large as 110 μm were present. In addition to these rare large crystals, about 20 L^{-1} smaller ($< 50 \mu\text{m}$) crystals were present in the 1 February TTL cirrus layer.

As discussed by Lawson et al. (2008), the largest CPI crystal images appear to be hexagonal plates, and analysis of the images indicates that the aspect ratios are about 6:1, with the possibility of somewhat larger aspect ratios due to uncertainty resulting from blur in the CPI images.

The altitude at which these large crystals are observed is surprising since they must fall as they grow by deposition of water vapor. Given the single-crystalline habits indicated by the images (see Fig. 1), it is implausible that these crystals are aggregates. Analysis of back trajectories from the flight path and infrared satellite imagery indicates that the air sampled had not been influenced by convection for several days. Since the residence time of these large crystals in the TTL is on the order of hours, they definitely were not produced by deep convection. Figure 3 shows the times to

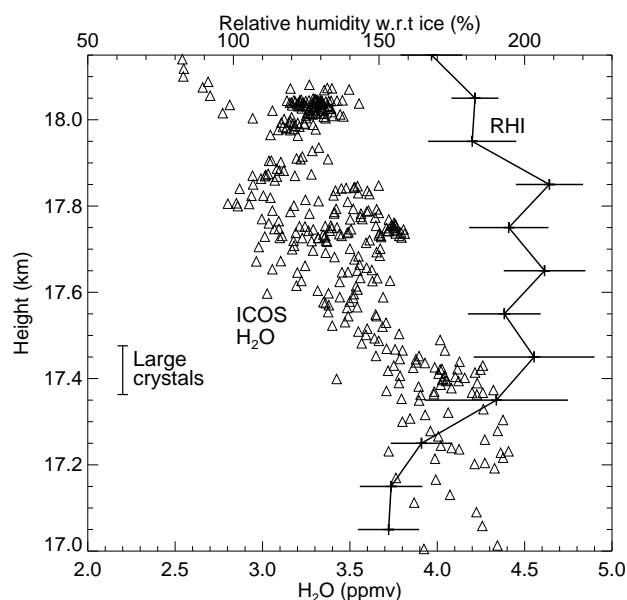


Fig. 4. Vertical profiles of WB-57 ICOS water vapor measurements (open triangles) made during the time period when the large ice crystals were detected. Corresponding relative humidities with respect to ice (using MMS temperature) are also shown (lines). The horizontal bars are one standard deviation. The precisions of the ICOS measurements is 0.14 ppmv; hence, the variability in water vapor concentrations is almost entirely geophysical.

grow spherical ice crystals of different sizes as well as the time to fall 500 m. We have chosen this distance for the sedimentation times because some of the large crystals were no more than about 500 m below $\approx 18.2 \text{ km}$ where temperature increases rapidly with height. For crystals larger than about 40–50 μm , the growth times exceed the sedimentation times (for the assumed humidity and relative humidity with respect to ice (RHI) of 3 ppmv and 140%, respectively). These calculations suggest that growth of the large crystals may require large supersaturations.

Water vapor was measured with multiple instruments on the WB-57 during the CRAVE flights. The Harvard water vapor (HWV) instrument photodissociates H_2O molecules with 121.6 nm (Lyman- α) radiation and detects the resulting OH photofragment fluorescence at 315 nm (Weinstock et al., 1994). Accuracy and precision for HWV on the 1 February flight were $\pm 5\%$ and 0.13 ppmv (for H_2O concentrations less than 10 ppmv), respectively. The Harvard ICOS (Integrated Cavity Output Spectroscopy) instrument uses a mid-infrared quantum cascade laser at 1484 cm^{-1} to obtain measurements of H_2O , as well as water vapor isotopes, with an effective path length of nearly 4 km (Sayres, 2006). The accuracy and precision of the ICOS instrument are 5% and 0.14 ppmv, with a potential bias of $\pm 0.25 \text{ ppmv}$. Figure 4 shows vertical profiles of water vapor and RHI from the ICOS instrument for the time-period on 1 February when the large ice crystals

were detected. (The HWV water vapor concentrations were about 0.5 ppmv higher than the ICOS values for the segment of the 1 February flight during which the TTL cirrus was sampled.) At altitudes above about 17.4 km where the ice crystal growth must have occurred, the ICOS measurements indicate water vapor concentrations of about 3–4 ppmv, corresponding to RHI values around 200% given the low temperatures.

The measurements of RHI values of $\approx 200\%$ within cirrus clouds should not be taken as evidence the ice crystals are in steady-state with the large supersaturations. These are extremely tenuous cirrus clouds, and the time-scale for quenching of supersaturation is hours. Also, if the ice crystals were in quasi-equilibrium with the large ambient supersaturation, then the growth of the large crystals would simply not be possible.

A longstanding discrepancy between the aircraft water measurements and frostpoint balloon measurements in the stratosphere (with the aircraft instrument water concentrations considerably larger than the frostpoint values (Oltmans and Rosenlof, 2000)) has yet to be resolved. One of the CRAVE objectives was to make extensive comparisons between balloon-borne frostpoint hygrometer measurements and the WB-57 water vapor measurements. Nearly every WB-57 flight ended with the aircraft spiraling down over the airport, coordinated with frostpoint balloon sonde launches, such that they were sampling the tropopause region at approximately the same location and time. The frostpoint and aircraft water vapor measurements from the 1 February spiral are shown in Fig. 5. The discrepancy is quite large, with the HWV and ICOS instruments indicating ≈ 3 –4 ppmv near the tropopause, and the frostpoint instrument indicating 1–2 ppmv. Comparisons from other flights indicate that the frostpoint measurements systematically indicate that the TTL is about 1–2 ppmv drier than do the Harvard measurements.

The unresolved discrepancy between the various in situ instruments measuring water vapor in the upper troposphere and lower stratosphere presents a problem for validation of satellite water vapor measurements. Included in Fig. 5 are Aura Microwave Limb Sounder (MLS) water vapor retrievals (version 1.5) within 24 h of the spiral descent and $\pm 10^\circ$ latitude/longitude of the San Jose airport. The MLS H_2O retrievals are in much better agreement with the frostpoint balloon measurements than with the HWV and ICOS measurements.

3 Growth-sedimentation calculations

We begin by using simple growth-sedimentation calculations to investigate the formation of the large crystals. Our approach is to start with the observed crystal size and location and integrate backwards in time. Thus, the crystals get smaller (due to reverse deposition of ice) and ascend (due

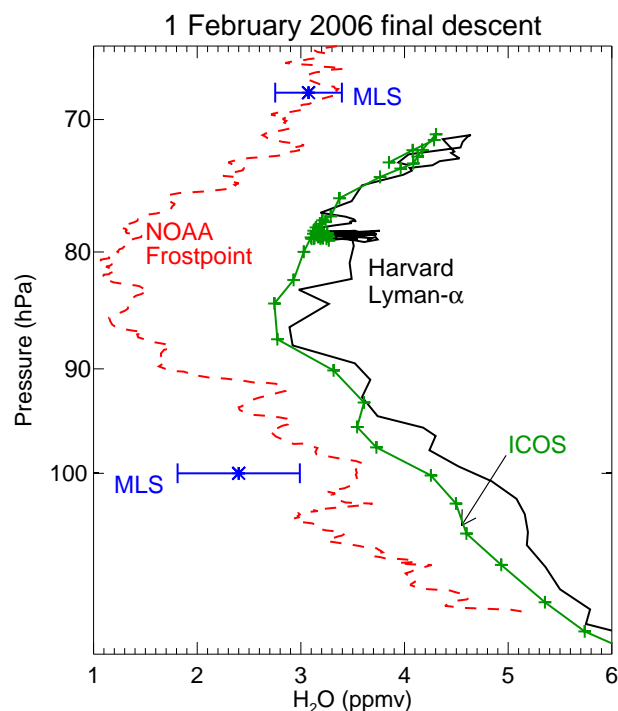


Fig. 5. Water vapor measurements from the WB-57 Harvard water vapor instrument (black solid) and ICOS (green with + symbols) made during a spiral descent over San Jose are compared with the coordinated frostpoint balloon measurements (red dashed). The measurements differ by 1–2 ppmv, with the frostpoint instrument indicating much lower water concentrations than the HWV and ICOS in the tropopause region. Also shown are the MLS water vapor retrievals within ± 1 day and $\pm 10^\circ$ latitude/longitude of the spiral. The MLS values are in good agreement with the frostpoint sonde measurements.

to reverse sedimentation) as the calculation proceeds. We continue until the particle size goes to zero, which would be the location and time where nucleation occurred, or until the crystal ascends into the stratosphere where the temperature is high enough such that the RHI drops below 100% and the crystal begins to get larger (in reverse time). In the latter case, the crystal would indefinitely rise and grow in the subsaturated stratosphere, thus we argue that the calculation failed to explain the existence of the crystal.

Breon and Dubrulle (2004) showed that even relatively small hexagonal-plate ice crystals can be nearly oriented. Specifically, they showed that for moderate turbulence levels, hexagonal plates as small as $15\ \mu\text{m}$ will have their basal axes within about 10° of the vertical. To obtain the minimum fallspeed, we calculate sedimentation speeds assuming the crystals are perfectly oriented plates. Shape corrections for fallspeeds based on oblate spheroids given by Fuchs (1964) are used. These expressions indicate fallspeeds for perfectly oriented plates as much as 40% lower than for equivalent-volume spheres for aspect ratios as large as 10.

Table 1. Factors controlling crystal growth rates. In each case, assumptions were made that minimize the water vapor concentration required to grow the large crystals.

Issue	Assumption	Impact on crystal growth
Deposition coefficient	Unity	Fastest possible growth
Nucleation threshold	$\text{RHI} \simeq 100\%$	Deepest possible supersaturated layer
Crystal temperature	$T_{\text{ice}} = T_{\text{amb}}$	Fastest growth
Ice phase (cubic/hexagonal)	Hexagonal	Fastest growth
Crystal habit	Thin plate	Minimum volume, slow sedimentation
Crystal orientation	Horizontally oriented	Slowest sedimentation
Crystal growth shape effect	Capacitance model	Fastest growth

Ice crystal deposition growth rates are calculated following Toon et al. (1989). For crystal sizes larger than about $10\text{ }\mu\text{m}$ at TTL temperatures and pressures, the growth rate is limited by diffusion of vapor toward the crystal. We model the crystal growth of the hexagonal plates using the traditional capacitance analogy to electrostatic theory. Capacitances for the growth calculations are taken from recent numerical calculations for growth of hexagonal plates (Chiruta and Wang, 2005).

Calculation of capacitance involves solving the Laplace equation for vapor density around the ice crystal and vapor flux to the ice crystal with the boundary conditions of $p_{\text{vap}} = p_{\text{sat}}$ at the crystal surface and $p_{\text{vap}} = p_{\text{vap},\infty}$ at a large distance from the crystal, where p_{sat} is the saturation vapor pressure over ice and $p_{\text{vap},\infty}$ is the ambient H_2O vapor pressure. These boundary conditions imply an assumption that water molecules impinging anywhere on the crystal have equal probability of getting incorporated into the ice lattice before desorption. In the case of an extremely thin plate, growth is primarily only occurring on the prism faces, and the above assumption implies that water molecules adsorbing on the basal faces can rapidly diffuse (up to 10 s of microns) on the surface before they desorb. Hence, the capacitance model provides an upper limit for the linear growth rate of high aspect ratio crystals. If, in reality, water molecules did not readily diffuse across ice crystal surfaces before desorbing, the growth rate would be slower.

It is worth noting here that if growth occurred only via molecules adsorbing on the prism faces, then the rate of increase of the crystal maximum dimension would be approximately the same as it would be for an equidimensional crystal. Based on the calculations presented below, growth of the large crystals would not be possible if they were equidimensional; water vapor concentrations exceeding 10 ppmv would be required. The implication here is that water molecules must readily diffuse across the crystal surfaces.

For a particular crystal size and aspect ratio, we calculate the plate thickness. Then as the reverse-time growth calculation proceeds, we assume the plate thickness does not change until the length decreases to the thickness. Thereafter, we as-

sume the equidimensional crystal grows like a sphere. This approach is consistent with the fact that smaller CPI crystal images appear more equidimensional (Lawson et al., 2008).

In addition to using the capacitance model for calculating crystal growth rates and assuming perfect orientation for sedimentation calculations, we make several other assumptions here that should maximize crystal growth (see Table 1). The deposition coefficient is assumed to be unity regardless of the ice supersaturation. Using a substantially lower deposition coefficient would slow crystal growth. Also, Wood et al. (2001) argued that using the capacitance model for calculations of hexagonal crystal growth overestimates the growth rate by about 10–15%. We assume the crystal temperature is equal to the ambient temperature. In reality, the crystals could be warmer than the environment due to absorption of infrared radiation from the warm surface below. If the crystals were substantially warmer, then the equilibrium vapor pressure would be higher, thus limiting growth. We assume water vapor is not depleted by the growing crystals. We do not impose any supersaturation threshold for nucleation of the crystals, thus maximizing the depth of the layer in which they can grow. We assume the crystals are composed of hexagonal ice instead of cubic ice. The vapor pressure over cubic ice is about 10% higher than that over hexagonal ice (Shilling et al., 2006), thus cubic ice will grow slower than hexagonal ice. If we did not make these assumptions, it would be more difficult to grow the large crystals, and even more water vapor would be required to grow them.

We assume a temperature profile based on the measured temperature versus altitude on the 1 February flight (green curve in Fig. 2). For altitudes above those sampled during the TTL cirrus sampling period, we use the highest cold-point tropopause (at $\simeq 77\text{ hPa}$) on the 1 February flight. We assume here that the temperature profile does not change upstream of the observation location. National Centers for Environmental Prediction (NCEP) analyses do not suggest that the tropopause was higher and colder upstream (to the west) of the flight track. The impact of gravity wave driven temperature and vertical wind perturbations are addressed in Sect. 4. Simulations are run assuming vapor mixing ratios (constant

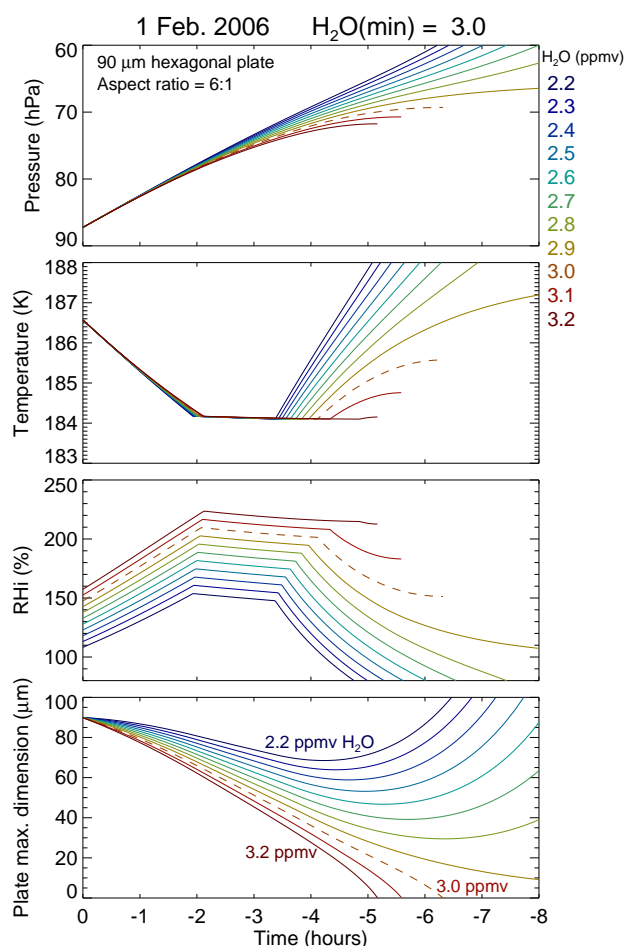


Fig. 6. Calculated history of pressure, temperature, ice relative humidity, and crystal maximum dimension (length of basal face) for a 90- μm plate with an assumed aspect ratio of 6:1. We are tracing the crystal evolution back in time; as a result, the crystals ascend (due to sedimentation) and shrink (due to deposition growth in supersaturated air) as the calculation proceeds. The colors indicate the water vapor mixing ratio assumed. Only if the water vapor concentration is at least 3.0 ppmv (dashed curves) does the crystal diameter shrink to zero before the particle reaches subsaturated air in the stratosphere.

in altitude) ranging from 1 to 6 ppmv. The corresponding ice relative humidities can be quite large ($>200\%$ for mixing ratios greater than about 3 ppmv).

Examples of the reverse-time growth-sedimentation calculations are shown in Fig. 6. For this case, we assume a 90- μm hexagonal plate and an aspect ratio of 6:1. Again, since we are tracing the observed crystal back toward its origin, deposition growth and sedimentation are reversed: the crystal rises and shrinks (while in supersaturated air) as the calculation proceeds. For this particular crystal, the calculated size shrinks to zero (the point of nucleation) before it rises into subsaturated air in the stratosphere only if the water vapor mixing ratio is at least ≈ 3.0 ppmv. We argue that,

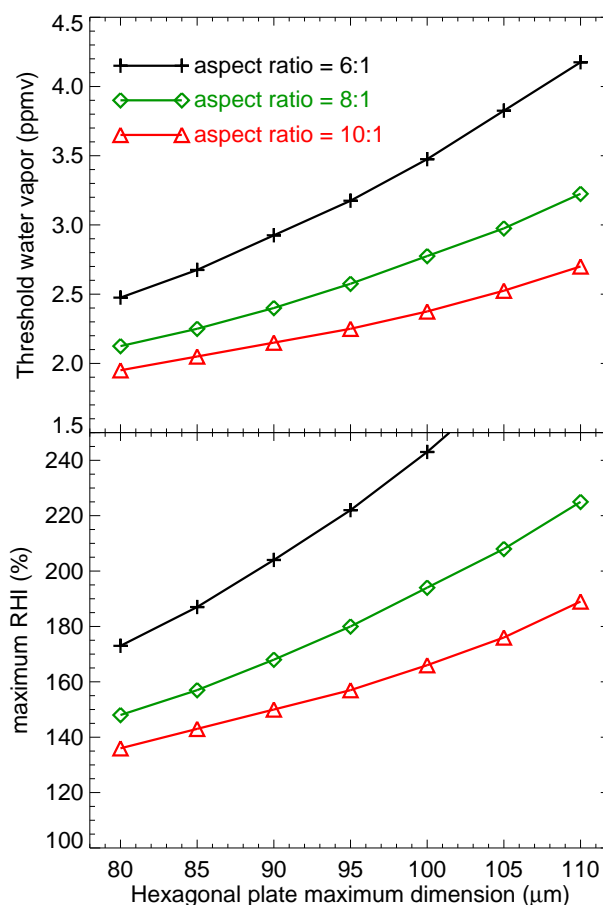


Fig. 7. Results from growth-sedimentation calculations are shown. Threshold water vapor mixing ratio (top panel) and maximum RHI (bottom panel) are plotted versus hexagonal plate maximum dimension for three different aspect ratios. See text for details.

given the assumptions made about temperature profile, vertical wind ($w=0$ in this case), and crystal aspect ratio=6:1, the existence of this 90- μm crystal implies that the water vapor mixing ratio in the tropopause region must have been at least about 3.0 ppmv. The peak RHI reached in the simulation with 3.0 ppmv of H_2O is about 200%.

The threshold water vapor concentrations and maximum RHIs are very sensitive to the crystal aspect ratio assumed (see Fig. 7). If the aspect ratios are on the low end indicated by the image analysis ($\approx 6:1$) (Lawson et al., 2008), then growth of the 90–100 μm crystals would require TTL water vapor concentrations of about 3–3.5 ppmv that are in good agreement with the ICOS measurements. Growth of a 110 μm crystal would require more water (≈ 4 ppmv) than even the ICOS measurements indicated, and the corresponding maximum relative humidity would be in excess of saturation with respect to liquid water. If the aspect ratios are as large as 8:1, then the 90–100 μm crystals could be grown with water vapor mixing ratios of ≈ 2.4 –2.7 ppmv that are

somewhere between the ICOS and frostpoint values. On the other hand, if the aspect ratios are much larger ($\geq 10:1$), then water vapor concentrations closer to the low end of the measurement range (≈ 2.0 – 2.5 ppmv) would suffice to grow the large crystals. Note that this analysis only provides a lower limit to the water concentrations. Also, if the crystals were actually equidimensional, an implausible water vapor concentration of more than 10 ppmv would be required to grow even an $80\text{ }\mu\text{m}$ crystal.

4 Influence of gravity waves

Since the size of crystals near the tropopause is limited by a competition between deposition growth and sedimentation, it seems likely that upward vertical motion could allow larger crystals to grow by lofting them in the narrow supersaturated layer. The mean upward motion in balance with radiative heating near the tropopause is very weak ($\approx 0.3\text{ mm s}^{-1}$ (Rosenlof, 1995)) and has negligible effect on the growth of large crystals. However, gravity waves are commonly observed near the tropical tropopause and can drive substantial vertical motions as well as temperature perturbations (Pfister et al., 1993; Alexander and Pfister, 1995; Tsuda et al., 2000).

We investigate the impact of waves on formation of the large TTL crystals by repeating the growth-sedimentation calculations with superimposed wave-driven temperature and vertical wind perturbations using a plausible range of wave amplitudes and frequencies. We use intrinsic periods ranging from 4 to 32 h and net vertical displacements up to $\approx 450\text{ m}$. The corresponding vertical wind speed and temperature perturbations are at most about 10 cm s^{-1} and 4 K, respectively. Even though very little convection was present near the flight track, the group velocity of the low-frequency waves is inclined 80–90 degrees from the zenith; hence, they can propagate long horizontal distances.

The vertical wind and temperature perturbations are simply represented as a sinusoidal function of time and altitude, with temperature leading vertical velocity by one quarter cycle. For each intrinsic frequency and amplitude, we run the simulations for a range of phases between 0 and 2π . The greatest enhancement of crystal growth occurs when the maximum upward motion from the wave corresponds to the time when the crystal is largest and is falling the fastest.

For this analysis we use a crystal with a length of $100\text{ }\mu\text{m}$, and we assume an aspect ratio of 8:1. Table 2 shows the results of growth-sedimentation calculations for the range of wave frequencies and amplitudes assumed. The threshold water vapor concentrations and peak relative humidities correspond to the simulation with the wave phase that results in minimum threshold water vapor. The wave-driven temperature perturbations superimposed on an already cold temperature profile result in very large relative humidities. We consider relative humidity with respect to liquid water substantially exceeding 100% to be non-physical because nu-

merous water drops would rapidly activate and freeze followed by rapid depletion of vapor in excess of ice saturation. Hence, we exclude simulations for which the wave temperature perturbation drives substantial supersaturation with respect to liquid water. For the vapor pressure with respect to liquid water, we use the expression given by Clegg and Brimblecombe (1995). Given the uncertainty in the saturation vapor pressure of water at these low temperatures, we only exclude simulations for which the peak relative humidity exceeds 120%. At 185 K, this limit corresponds to an RHI of about 240%.

High-frequency gravity waves have negligible impact on the threshold water vapor concentration. However, as discussed above, these waves do increase the maximum RHs experienced by the crystals as they fall through the TTL. For example, superimposing a 4-h wave with a 1.1-K temperature amplitude increases the maximum RHI from 196% (with no wave) to 240%. Increasing the wave amplitude further would result in relative humidities with respect to liquid water above the 120% limit discussed above. The longest period (32 h) waves considered do decrease the threshold water vapor and maximum relative humidity (i.e., to 2.6 ppmv and 187% for a wave amplitude of 1.1 K). However, if we increase the wave amplitude further, then, again, we start to get larger peak relative humidities.

We find that regardless of assumptions about aspect ratio and vertical wind, it would be impossible to grow the crystals as large as $100\text{ }\mu\text{m}$ if the TTL water vapor in the crystal growth region were less than 2 ppmv. Even with an assumed aspect ratio of 14:1 and a constant upward motion of 2 cm s^{-1} , at least 2 ppmv H_2O is required to grow the $100\text{-}\mu\text{m}$ crystals. However, it is possible that the water vapor concentration was higher upstream and growth of the TTL cirrus ice crystals removed vapor in excess of saturation. This issue is discussed further below.

5 Implications for ice nucleation

The growth-sedimentation calculations in the previous sections suggest that if the crystals are not extremely thin plates (aspect ratios $>8:1$) then ice supersaturations within the TTL cirrus must be surprisingly large ($\text{RHI} \geq 190\%$) to allow the growth of $\approx 100\text{ }\mu\text{m}$ crystal. Past modeling studies (e.g. Jensen and Pfister, 2004) have generally assumed that the primary mechanism for nucleation of ice crystals in the upper troposphere is homogeneous freezing of aqueous sulfate aerosols. Within this context, such large supersaturations defy expectations. Laboratory investigations of aerosol freezing indicate that ice nucleation occurs very rapidly when the RHI exceeds about 160–170% (Koop et al., 2000). An ample supply of aerosols (presumed to be aqueous sulfate) is always present in the upper troposphere, and freezing of these aerosols followed by deposition of vapor on the ice crystals would prevent the supersaturation from

Table 2. Results from growth-sedimentation simulations with gravity waves (crystal length = 100 μm , aspect ratio = 8:1).

Intrinsic period (hours)	Vertical wind amplitude (cm s^{-1})	Temperature amplitude ^a (K)	Maximum vertical displacement (m)	Minimum H ₂ O thresh (ppmv)	Maximum RHI (%) ^b
no wave	n/a	n/a	n/a	2.8	196
4	2.5	0.6	60	2.8	209
4	5	1.1	110	2.8	240
8	1.25	0.6	60	2.8	184
8	2.5	1.1	110	2.8	192
16	1.25	1.1	110	2.7	232
16	2.5	2.1	220	2.8	207
32	0.625	1.1	110	2.6	187
32	1.25	2.1	220	2.7	198
32	2.5	4.2	450	3.3	234

^a The temperature perturbation experienced by the cloud particle.

^b The maximum RHI encountered in the simulation with the ideal wave phase.

exceeding the RHI threshold for freezing by more than several % (Kärcher and Lohmann, 2002). Modeling studies have shown that the concentration of ice crystals produced by homogeneous freezing of aqueous aerosols is primarily controlled by cooling rate (Jensen and Toon, 1994; Kärcher and Lohmann, 2002). Even with relatively slow, synoptic-scale cooling, ice concentrations should far exceed those observed in the CRAVE TTL cirrus ($\approx 20\text{--}100\text{ L}^{-1}$) and the deposition of water vapor on the numerous crystals would rapidly deplete the supersaturation to values well below those required to grow the large crystals.

The existence of very large ice supersaturations and the apparent discrepancy with laboratory measurements of aerosol freezing was discussed by Jensen et al. (2005b). Brief measurements of RHI values exceeding 200% from WB-57 flights out of Costa Rica during January 2004 were presented, and three possible explanations were discussed: (1) the expressions used for calculating vapor pressure over supercooled water at low temperatures give values that are at least 20% too low, (2) organic films on the aerosol surfaces reduce their accommodation coefficient for uptake of water, resulting in aerosols with more concentrated solutions when moderate-rapid cooling occurs and correspondingly inhibited homogeneous freezing, and (3) if surface freezing dominates, organic coatings may increase the surface energy of the ice embryo/vapor interface resulting in suppressed ice nucleation. The potential impact of organics on aerosol freezing was also discussed by Kärcher and Koop (2005).

For investigation of potential scenarios permitting growth of large crystals, we use detailed simulations of ice nucleation, growth, sedimentation, and exchange of water between the vapor and condensed phases to quantify the constraints on nucleation imposed by the existence of large crystals. Specifically, we use the Lagrangian model described by Jensen and Pfister (2004) that tracks the growth and sedimentation of thousands of individual ice crystals in a vertical column. For

calculation of water vapor concentrations, we use an Eulerian vertical grid with potential temperature as the vertical coordinate. The vertical domain and grid spacing are $\theta=360\text{--}440\text{ K}$ and $d\theta=0.2\text{ K}$. This model was previously used to simulate TTL cirrus sampled in the subtropics (Jensen et al., 2005a). A deposition coefficient of unity is assumed to maximize crystal growth rates. As in the calculations above, sedimentation is modeled assuming the crystals are thin hexagonal plates (aspect ratio=8:1). Ice crystal aggregation is neglected, but as discussed above, the hexagonal plate crystals observed are apparently not aggregates. The Koop et al. (2000) parameterization is used to calculate aerosol freezing ice nucleation rates as a function of water activity.

Following the approach previously used (Jensen et al., 2005b), we run idealized simulations with a specified cooling rate and a final profile as specified in Fig. 2. We use an initial H₂O mixing ratio of 3 ppmv, and we start the simulation far enough upstream such that the initial RHI is everywhere less than 100%.

We first investigate the typically assumed scenario in which ice nucleation occurs via homogeneous freezing of aqueous sulfate aerosols. The initial aerosol size distribution in the simulation is based on the mean of the size distributions measured by the Nucleation-Mode Aerosol Size Spectrometer (N-MASS) (Brock et al., 2000) and Focused Cavity Aerosol Spectrometer (FCAS) (Jonsson et al., 1995) instruments for the time period on 1 February. The results given here are not sensitive to the assumed aerosol size distribution. The mass accommodation coefficient for uptake of water by the aqueous aerosols is assumed to be 0.1, such that the aerosols can take up water relatively quickly, and they essentially stay in equilibrium with the environmental water vapor as relative humidity changes.

With a synoptic-scale cooling rate of 0.6 K hr^{-1} (equivalent to an updraft speed of 1.7 cm s^{-1}), homogeneous freezing of sulfate aerosols produces ice concentrations of

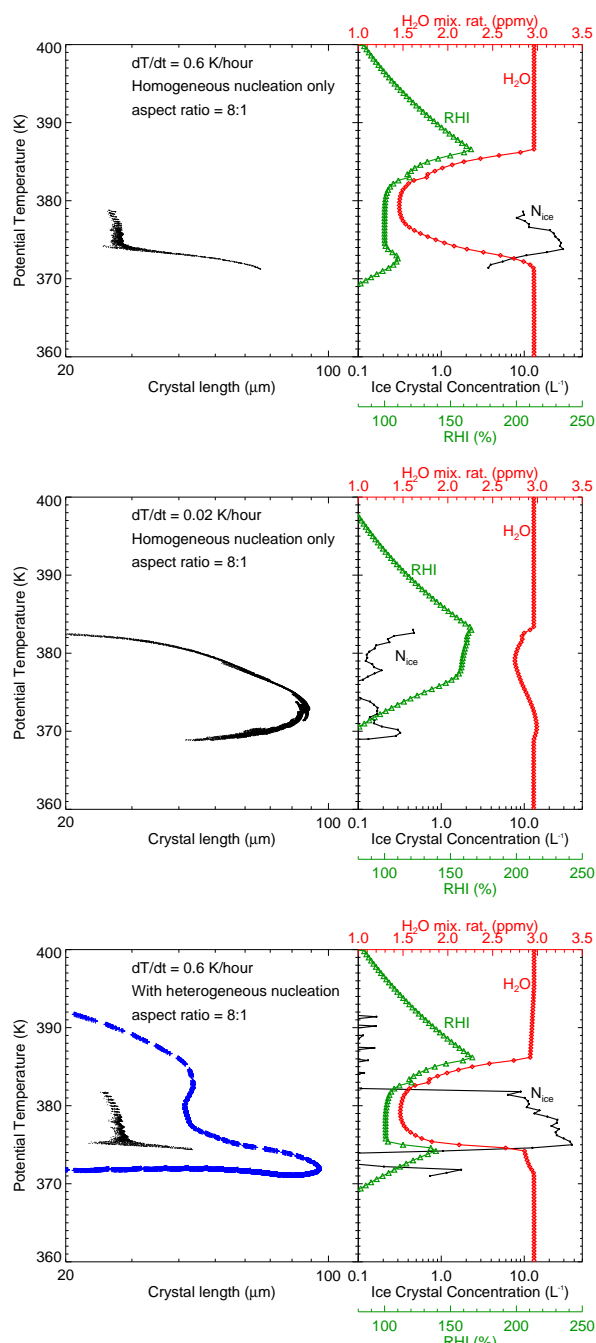


Fig. 8. Results from TTL cirrus simulations with a detailed cloud model are shown. The different panels are (a) cooling rate = 0.6 K hr^{-1} and no heterogeneous ice nuclei, (b) cooling rate = 0.02 K hr^{-1} and no heterogeneous ice nuclei, and (c) cooling rate = 0.6 K hr^{-1} and including ice nuclei active at about 8% ice supersaturation. The left panels show individual ice crystal lengths and potential temperatures. The curves in the right panels are water vapor mixing ratio (red), RHI (green), and ice concentration (black). In the bottom panel, homogeneously-nucleated and heterogeneously-nucleated crystals are shown as black points and blue points, respectively. Results are shown at the time when the maximum crystal size occurred.

$\approx 20 \text{ L}^{-1}$. Growth of these ice crystals drives down the RHI to near saturation (corresponding to H_2O concentrations as low as about 1.5 ppmv near the temperature minimum) within the cloud, effectively limiting the growth of large crystals. The maximum crystal size in this simulation is about $65 \mu\text{m}$ (see Fig. 8a), which is considerably smaller than the observed crystal lengths of $90\text{--}110 \mu\text{m}$.

Assuming slower cooling rates results in fewer ice crystals nucleating and less competition for vapor. With a very slow cooling rate of 0.02 K hr^{-1} (0.5 mm s^{-1}), ice concentrations are limited to no more than about 1 L^{-1} . Growth of these crystals limits the RHI to about 170%, but does not drive it down to ice saturation (see Fig. 8b). Water vapor concentrations are only depleted by about 0.5 ppmv . As a result, at pressures lower than 90 hPa (i.e., altitudes at or above where the large crystals were observed), the crystals grow as large as $90 \mu\text{m}$.

The extremely slow cooling scenario is unsatisfactory for two reasons. First, temperature variability driven by gravity waves is essentially ubiquitous in the tropics. It is extremely improbable that nucleation events driven by cooling rates larger than 0.02 K hr^{-1} would not occur. The MMS temperature measurements from the 1 February flight indicate the presence of high-frequency temperature variability typical of the tropical tropopause region. Second, the ice concentrations in the slow cooling simulation ($<1 \text{ L}^{-1}$) are far lower than the ice concentrations indicated by the 2D-S and CAPS measurements. In the 1 February TTL cirrus cloud, the ice concentrations were about $20\text{--}30 \text{ L}^{-1}$, and the mean TTL cirrus ice concentration for the entire mission was about 65 L^{-1} (Lawson et al., 2008).

A further assumption we can make is that the large crystals were produced by very effective heterogeneous ice nuclei (IN) active at low ice supersaturation. Given the very low concentrations of large crystals in the TTL cirrus, this assumption is not unreasonable. DeMott et al. (2003) showed that low concentrations ($1\text{--}10 \text{ L}^{-1}$) of ice nuclei active at RHIs as low as 115% are typically present in the northern hemisphere mid-latitude free troposphere. Allowing a small number of ice crystals to nucleate on effective ice nuclei essentially deepens the layer in which the crystals can grow. Figure 8c and d show the results of including 0.1 L^{-1} ice nuclei that activate at RHI of about 108% in a simulation with a cooling rate of 0.6 K hr^{-1} . Growth of the 0.1 L^{-1} heterogeneously nucleated ice crystals does not substantially deplete the water vapor. Hence, these ice crystals can grow to large sizes before the onset of homogeneous aerosol freezing results in more numerous ice crystals that deplete the vapor. The net result is a few crystals approaching $100 \mu\text{m}$ and about 20 L^{-1} smaller ice crystals generated by homogeneous nucleation.

Note that the cloud simulation shown in Fig. 8c indicating extreme dehydration within the homogeneously-nucleated ice crystal layer is inconsistent with the Harvard Water Vapor and ICOS measurements indicating about 3 ppmv and large

supersaturations throughout the TTL cirrus layer. The WB-57 measurements from other CRAVE flights also provide no clear evidence of dehydration within the TTL cirrus. If the balloon-borne frostpoint measurements are correct, then it is possible there was more water vapor upstream of the TTL cirrus layers, and the clouds depleted the vapor mixing ratio down to ≈ 2 ppmv.

Consistent with the growth-sedimentation calculations discussed above, if we start the simulation with only 2 ppmv of water vapor, the heterogeneously nucleated ice crystals only grow to about $62\text{ }\mu\text{m}$, and we cannot explain the larger observed crystals. In this simulation, the RHI never gets large enough for homogeneous freezing, and there is no significant depletion of vapor.

6 Conclusions

We have used simple growth-sedimentation calculations as well as full cloud simulations to investigate the formation of relatively large crystals at the tropical tropopause. We now discuss the implications of these calculations in the context of the discrepancies in TTL water vapor measurements amongst the various CRAVE instruments. As discussed in Sect. 2, the Harvard Water Vapor and ICOS instruments indicate 3–4 ppmv H_2O concentrations in the TTL for the 1 February flight we are focusing on, whereas the frostpoint and MLS measurements indicate <2 ppmv. The uncertainty in the hexagonal plate aspect ratios leaves a range of possibilities. If the aspect ratios are comparable to the lower limits indicated by analysis of the CPI images ($\approx 6:1$) then water vapor concentrations on the high end of the measurement range (>3 ppmv) are required to grow the large crystals. On the other hand, if the aspect ratios are considerably larger ($\geq 10:1$), then water vapor concentrations (≈ 2 – 2.3 ppmv) that are closer to the lower values indicated by the frostpoint and MLS measurements would be sufficient to grow the large crystals. If we instead assume the water vapor measurements on the lower end of the measurement range are correct, and if considerably more water vapor was not available for crystal growth upstream, the implication is that the crystals necessarily have very large aspect ratios.

We find that it would not be possible to grow the large crystals if the water vapor concentration in the crystal growth region were <2 ppmv. Even with aspect ratios of 15 and 2 cm s^{-1} upward motion to loft the crystals, we still need more than 2 ppmv to grow the crystals. We cannot rule out the possibility that upstream of the location where the crystals were observed, higher water vapor mixing ratios prevailed, and the TTL humidity was reduced by growth of the TTL cirrus crystals. The mean ice water content in the cirrus layer observed on 1 February was ≈ 0.25 ppmv, but the cloud could have contained more condensed water at an earlier time. Also, the cloud was very patchy, and the peak ice water content was >2 ppmv. An important caveat is that the

crystals grew and sedimented in a sheared, three-dimensional flow. Hence, it is possible that the air mass that the crystals grew in had very different water vapor concentrations than the air mass sampled by the WB-57.

Detailed simulations of the TTL cirrus formation show that the observations of a small number of large crystals as well as $\approx 20\text{ L}^{-1}$ smaller crystals are difficult to reconcile if homogeneous freezing of aqueous aerosols is the only source of ice crystals. If the cooling rate is rapid enough to generate ice concentrations as large as 20 L^{-1} , then the crystals rapidly deplete the vapor in excess of saturation, and growth of large crystals is prevented. The presence of a low concentration of very effective heterogeneous ice nuclei could permit production of ice crystals at low supersaturations. These crystals could grow large before the onset homogeneous nucleation and the subsequent dehydration.

The CRAVE subvisible cirrus observations remain puzzling for two reasons. First, the ice concentrations were relatively low (mean= 66 L^{-1} , maximum= 166 L^{-1}) (Lawson et al., 2008). Given the high-frequency temperature variability typical of the tropical tropopause region, it is surprising that higher ice concentrations were not present in some locations. Second, the water vapor observations show no clear evidence of dehydration in the subvisible cirrus layers. The simulations presented here suggest that, even with the observed low ice concentrations, significant dehydration would be expected.

As discussed by Jensen and Pfister (2005), the possibility that substantial ice supersaturation can be maintained within cold TTL cirrus has implications for our understanding of dehydration as air ascends through the TTL into the stratosphere. In particular, the in-cloud supersaturation would allow about 0.5–1 ppmv higher H_2O concentrations in air entering the stratosphere than if the clouds could dehydrate air down to ice saturation. This scenario contrasts sharply with the general assumption made in trajectory modeling studies that all vapor in excess of ice saturation gets removed as air passes through the cold tropopause region. Hence, a better understanding of the cloud processes is required to develop a quantitative relationship between tropopause temperatures and the concentration of water vapor in air entering the stratosphere. Resolution of the water vapor measurement discrepancies is a necessary step toward making progress on these issues.

Acknowledgements. This work was supported by NASA's Radiation Science Program and the Aura Validation Program. We are grateful for helpful discussions with D. Murphy and Ru-Shan Gao. We also thank B. Read for providing the MLS water vapor data.

Edited by: T. Koop

References

- Alexander, M. and Pfister, L.: Gravity wave momentum flux in the lower stratosphere over convection, *Geophys. Res. Lett.*, 22, 2029–2032, 1995.
- Baumgardner, D., Jonsson, H., Dawson, W., Connor, D. O., and Newton, R.: The cloud, aerosol and precipitation spectrometer (CAPS): A new instrument for cloud investigations, *Atmos. Res.*, 59, 59–60, 2001.
- Breon, F.-M. and Dubrulle, B.: Horizontally oriented plates in clouds, *J. Atmos. Sci.*, 61, 2888–2898, 2004.
- Brock, C. A., Schroeder, F., Kärcher, B., Petzold, A., Busen, R., and Fiebig, M.: Ultrafine particle size distributions measured in aircraft exhaust plumes, *J. Geophys. Res.*, 105, 26 555–26 567, 2000.
- Chiruta, M. and Wang, P. K.: The capacitance of solid and hollow hexagonal ice columns, *Geophys. Res. Lett.*, 32, L05803, doi:10.1029/2004GL021771, 2005.
- Clegg, S. L. and Brimblecombe, P.: Application of a multicomponent thermodynamic model to activities and thermal properties of 0–40 mol kg⁻¹ aqueous sulfuric acid from <200 to 328 K, *J. Chem. Eng. Data*, 40, 43–64, 1995.
- Comstock, J. M., Ackerman, T. P., and Mace, G. G.: Ground based remote sensing of tropical cirrus clouds at Nauru Island: Cloud statistics and radiative impacts, *J. Geophys. Res.*, 107, 4714, doi:10.1029/2002JD002203, 2002.
- DeMott, P. J., Cziczo, D. J., Prenni, A. J., Murphy, D. M., Kreidenweis, S. M., Thomson, D. S., and Borys, R.: Measurements of the concentration and composition of nuclei for cirrus formation, *Proc. of National Acad. Sci.*, 100, 14 655–14 660, 2003.
- Dvorstov, V. L. and Solomon, S.: Response of the stratospheric temperatures and ozone to past and future increases in stratospheric humidity, *J. Geophys. Res.*, 106, 7505–7514, 2001.
- Fuchs, N. A.: The mechanics of aerosols, General Publishing Company, 35–36, 1964.
- Fueglistaler, S., Bonazzola, M., Haynes, P. H., and Peter, T.: Stratospheric water vapor predicted from the Lagrangian temperature history of air entering the stratosphere in the tropics, *J. Geophys. Res.*, 110, D08107, doi:10.1029/2004JD005516, 2005.
- Gottelman, A., Randel, W. J., Wu, F., and Massie, S. T.: Transport of water vapor in the tropical tropopause layer, *Geophys. Res. Lett.*, 29, 1009, doi:10.1029/2001GL013818, 2002.
- Heymsfield, A. J.: Ice particles observed in a cirroform cloud at –85°C and implications for polar stratospheric clouds, *J. Atmos. Sci.*, 43, 851–855, 1986.
- Holton, J. and Gottelman, A.: Horizontal transport and dehydration of the stratosphere, *Geophys. Res. Lett.*, 28, 2799–2802, 2001.
- Jensen, E. J. and Pfister, L.: Transport and freeze-drying in the tropical tropopause layer, *J. Geophys. Res.*, 109, D02207, doi:10.1029/2003JD004022, 2004.
- Jensen, E. J. and Pfister, L.: Implications of Persistent Ice Supersaturation in Cold Cirrus for Stratospheric Water Vapor, *Geophys. Res. Lett.*, 32, L01808, doi:10.1029/2004GL021125, 2005.
- Jensen, E. J. and Toon, O. B.: Ice nucleation in the upper troposphere: Sensitivity to aerosol number density, temperature, and cooling rate, *Geophys. Res. Lett.*, 21, 2019–2022, 1994.
- Jensen, E. J., Toon, O. B., Pfister, L., and Selkirk, H. B.: Dehydration of the upper troposphere and lower stratosphere by sub-visible cirrus clouds near the tropical tropopause, *Geophys. Res. Lett.*, 23, 825–828, 1996.
- Jensen, E. J., Pfister, L., Bui, T.-P., Weinheimer, A., Weinstock, E., Smith, J., Pittmann, J., Baumgardner, D., and McGill, M. J.: Formation of a Tropopause Cirrus Layer Observed over Florida during CRYSTAL-FACE, *J. Geophys. Res.*, 110, L01808, doi:10.1029/2004JD004671, 2005a.
- Jensen, E. J., Smith, J. B., Pfister, L., Pitman, J. V., Weinstock, E. M., Sayres, D. S., Herman, R. L., Troy, R. F., Rosenlof, K., Thompson, T. L., Fridlind, A. M., Hudson, P. K., Cziczo, D. J., Heymsfield, A. J., Schmitt, C., and Wilson, J. C.: Ice supersaturations exceeding 100% at the cold tropical tropopause: implications for cirrus formation and dehydration, *Atmos. Chem. Phys.*, 5, 851–862, 2005b.
- Jonsson, H. H., Wilson, J. C., Brock, C. A., Knollenberg, R. G., Newton, R., Dye, J. E., Baumgardner, D., Borrmann, S., Ferry, G. V., Pueschel, R., Woods, D. C., and Pitts, M. C.: Performance of a focused cavity aerosol spectrometer for measurements in the stratosphere of particle size in the 0.06–2.0 µm diameter range, *J. Tech.*, 12, 115–129, 1995.
- Kärcher, B. and Koop, T.: The role of organic aerosols in homogeneous ice formation, *Atmos. Chem. Phys.*, 5, 703–714, 2005, <http://www.atmos-chem-phys.net/5/703/2005/>.
- Kärcher, B. and Lohmann, U.: A parameterization of cirrus cloud formation: Homogeneous freezing of supercooled aerosols, *J. Geophys. Res.*, 107, 4010, doi:10.1029/2001JD000470, 2002.
- Koop, T., Luo, B., Tsias, A., and Peter, T.: Water activity as the determinant for homogeneous ice nucleation in aqueous solutions, *Nature*, 406, 611–614, 2000.
- Korolev, A.: Reconstruction of the sizes of spherical particles from their shadow images. Part I: Theoretical considerations, *J. Atmos. Ocean. Tech.*, 24, 376–389, 2007.
- Lawson, R. P., Baker, B. A., Schmitt, C. G., and Jensen, T. L.: An overview of microphysical properties of Arctic clouds observed in May and July during FIRE ACE, *J. Geophys. Res.*, 106, 14 989–15 014, 2001.
- Lawson, R. P., O'Connor, D., Zmarzly, P., Weaver, K., Baker, B. A., Mo, Q., and Jonsson, H.: The 2D-S (Stereo) probe: Design and preliminary tests of a new airborne, high-speed, high-resolution imaging probe, *J. Atmos. Ocean. Tech.*, 23, 1462–1477, 2006.
- Lawson, R. P., Pilon, B., Baker, B., Mo, Q., Jensen, E., Pfister, L., and Bui, P.: Aircraft measurements of microphysical properties of subvisible cirrus in the tropical tropopause layer, *Atmos. Chem. Phys.*, 8, 1609–1620, 2008, <http://www.atmos-chem-phys.net/8/1609/2008/>.
- McFarquhar, G. M., Heymsfield, A. J., Spinhirne, J., and Hart, B.: Thin and subvisual tropopause cirrus: Observations and radiative impacts, *J. Atmos. Sci.*, 57, 1841–1853, 2000.
- Oltmans, S. J. and Rosenlof, K. H.: Data Quality, in: SPARC Assessment of Upper Tropospheric and Stratospheric Water Vapour, edited by: Kley, D., Russell, J. M., and Phillips, C., World Climate Research Program, 2000.
- Peter, T., Luo, B. P., Wernli, H., Wirth, M., Kiemle, C., Flentje, H., Yushkov, V. A., Khattatov, V., Rudakov, V., and S. Boormann, A. T., Toci, G., Mazzinghi, P., Beuermann, J., Schiler, C., Cairo, F., Don-francesco, G. D., Adriani, A., Volk, C. M., Strom, J., Noone, K., Mitev, V., MacKenzie, R. A., Carslaw, K. S., Trautmann, T., Santacesaria, V., and Stefanutti, L.: Ultrathin Tropical Tropopause Clouds (UTTCs): I. Cloud morphology and occurrence, *Atmos. Chem. Phys.*, 3, 1557–1578, 2003, <http://www.atmos-chem-phys.net/3/1557/2003/>.

- Pfister, L., Chan, K. R., Bui, T. P., Bowen, S., Legg, M., Gary, B., Kelly, K., Proffitt, M., and Starr, W.: Gravity waves generated by a tropical cyclone during the STEP tropical field program: a case study, *J. Geophys. Res.*, 98, 8611–8638, 1993.
- Rosenlof, K. H.: Seasonal cycle of the residual mean meridional circulation in the stratosphere, *J. Geophys. Res.*, 100, 5173–5191, 1995.
- Sayres, D. S.: New techniques for accurate measurement of water and water isotopes, Ph.D. Thesis, Harvard University, Cambridge, MA, 1–151, 2006.
- Shilling, J. E., Tolbert, M. A., Toon, O. B., Jensen, E. J., Murray, B. J., and Bertram, A. K.: Measurements of the vapor pressure of cubic ice and their implications for atmospheric ice clouds, *Geophys. Res. Lett.*, 33, L17801, doi:10.1029/2006GL026671, 2006.
- Solomon, S., Garcia, R. R., Rowland, F. S., and Wuebbles, D. J.: On the depletion of Antarctic ozone, *Nature*, 321, 755–758, 1986.
- Toon, O. B., Turco, R. P., Jordan, J., Goodman, J., and Ferry, G.: Physical processes in polar stratospheric ice clouds, *J. Geophys. Res.*, 94, 11 359–11 380, 1989.
- Tsuda, T., Nishida, M., and Rocken, C.: A global morphology of gravity wave activity in the stratosphere revealed by the gps occultation data (gps/met), *J. Geophys. Res.*, 105, 7257–7274, 2000.
- Weinstock, E. M., Hints, E. J., Dessler, A. E., Oliver, J. F., Hazen, N. L., Demusz, J. N., Allen, N. T., Lapsen, L. B., and Anderson, J. G.: New fast response photofragment fluorescence hygrometer for use on the NASA ER-2 and the Perseus remotely piloted aircraft, *Rev. Sci. Instrum.*, 22, 3544–3554, 1994.
- Wood, S. E., Baker, M. B., and Calhoun, D.: New model for the vapor growth of hexagonal crystals in the atmosphere, *J. Geophys. Res.*, 106, 4845–4870, 2001.